Geometric frustration in buckled colloidal monolayers

Y. Han[1,2,*], Y. Shokef[1,*], A. M. Alsayed[1], P. Yunker[1], T. C. Lubensky[1], and A. G. Yodh[1]

[1]*Department of Physics and Astronomy, University of Pennsylvania, 209 South 33rd St., Philadelphia, PA 19104, USA*

[2] *Department of Physics, Hong Kong University of Science and Technology, Clear Water Bay, Kowloon, Hong Kong*

$*$ *These authors contributed equally to this work.*

(Dated: September 24, 2008)

Abstract

Geometric frustration arises when lattice structure prevents simultaneous minimization of local interactions. It leads to highly degenerate ground states and, subsequently, complex phases of matter such as water ice, spin ice, and frustrated magnetic materials. Here we report a simple geometrically frustrated system composed of closely packed colloidal spheres confined between parallel walls. Diameter-tunable microgel spheres are self-assembled into a buckled triangular lattice with either up or down displacements analogous to an antiferromagnetic Ising model on a triangular lattice. Experiment and theory reveal single-particle dynamics governed by in-plane lattice distortions that partially relieve frustration and produce ground-states with zigzagging stripes and subextensive entropy, rather than the more random configurations and extensive entropy of the antiferromagnetic Ising model. This tunable soft-matter system provides an uncharted arena in which the dynamics of frustration, thermal excitations, and defects can be directly visualized.

Geometric frustration arises in physical and biological systems[1] ranging from water[2] and spin ice[3] to magnets[4,5], ceramics[6], and high-T_c superconductors[7]. The essence of this phenomenon is best captured in the model of Ising spins arranged on a two-dimensional (2D) triangular lattice and interacting anti-ferromagnetically[8,9]; two of the three spins on any triangular plaquette within this lattice can be antiparallel to minimize their anti-ferromagnetic (AF) interaction energy, but the third spin is *frustrated* because it cannot be simultaneously antiparallel to both neighbouring spins (Fig. 1A). Such frustration leads to materials with many degenerate ground states and extensive entropy proportional to the number of particles in the system. Consequently, small perturbations can introduce giant fluctuations with peculiar dynamics. Traditionally, these phenomena have been explored in atomic materials by ensemble averaging techniques such as neutron and X-ray scattering, muon spin rotation, nuclear magnetic resonance, and heat capacity and susceptibility measurements[5]. More recently, artificial arrays of mesoscopic constituents have been fabricated in order to probe geometric frustration at the single-'particle' level. Examples of the latter include Josephson junctions[10], superconducting rings[11], ferromagnetic islands[12–14], and recent simulations[15] of charged colloids in optical traps. Observations in these model systems, however, have been limited to the static patterns into which these systems freeze when cooled. Thus many questions about frustrated systems remain unexplored, particularly those associated with single-particle dynamics. For example, how, when, and why do individual particles change states to accommodate their local environments, and what kinetic mechanisms govern transitions to glassy phases?

Here we report on the static and *dynamic* properties of a self-assembled colloidal system analogous to Wannier's AF Ising model[8]. Densely packed spheres between parallel walls form an in-plane triangular lattice with out-of-plane up and down buckling[16–26]. The up-down states of the spheres produced by buckling are analogous to up-down states of Ising spins (Fig. 1B). Nearest-neighbour excluded volume interactions between particles favour opposite states for neighbouring particles, as do the AF interactions between neighbouring spins in the Ising model. In contrast to engineered mesoscopic systems[10–14], however, the colloidal system facilitates easy *tuning* of the effective AF interaction through changes in the diameter of temperature-sensitive microgel spheres[27]. The colloidal system also permits direct visualization of thermal motion at the *single-particle* level. In the limit of weak confinement, or weak interaction strength, system properties closely follow those predicted for the AF Ising model, but in the limit of strong confinement, they do not. For strong interactions, the lattice deforms to maximize free volume, and the collective na-

ture of the free-volume-dominated free energy characteristic of most soft-matter systems becomes important. We understand these effects theoretically in terms of tiling of the plane by isosceles triangles. The tiling scheme identifies a ground-state consisting of zigzagging stripes with sub-extensive entropy. Interestingly, in contrast to Ising-model predictions, first measurements of single-particle 'spin-flipping' suggest that flipping dynamics depend not only on the number of nearest-neighbour frustrated 'bonds', but on how these bonds are arranged. Thus the paper begins to explore connections between frustrated soft matter and hard materials such as frustrated AF media. (Unless otherwise specified, we use 'AF Ising Model' to refer to AF spins on a *rigid* triangular lattice; we will, however, also discuss this model on a deformable lattice.)

Experimental System. For walls separated by distances on order 1.5 sphere diameters, the particles maintain in-plane triangular order but buckle out-of-plane (Fig. 2, A, D). This buckling minimizes system free energy, $F = U - TS$, where U is the internal energy, T temperature, and S entropy. The bare interaction potential between our weakly charged[27] particles was measured to be short ranged and repulsive[28], i.e. nearly hard core. Thus the dominant contribution to the free energy is entropic. Spheres will move apart to minimize internal energy and to maximize their free volume (V) and entropy (proportional to ln$V$). This effect gives rise to multi-body effective interactions between spheres which, for low volume fractions, can be well approximated by a two-body repulsive entropic potential with range of order the interparticle spacing[29]. At high volume fraction many-body contributions to the potential may become important. The effective repulsion causes spheres to move to the top or bottom wall, and nearest-neighbours maximize free volume by moving to opposite walls (Fig. 1B). Buckled colloidal monolayers were first observed more than two decades ago[16–18], and the AF analogy was then suggested[17,30]. However, to date, few quantitative measurements have been performed on this system class, and the themes explored by most early work centred on structural transitions exhibited by colloidal thin films as a function of increasing sample thickness[17–20,22–24], rather than their connection to frustrated anti-ferromagnets. The use of temperature-sensitive *diameter-tunable* NIPA (N-isopropyl acrylamide) microgel spheres[27] also distinguishes our experiments from earlier work. By varying temperature we change particle size and sample volume fraction and, therefore, vary the strength of the effective AF interparticle interactions.

Samples were prepared at low volume fraction near the melting point to produce 2D crystal domains with $\sim 10^4$ spheres covering an area of order $(60\mu m)^2$. Video microscopy measurements were carried out far from grain boundaries on a $\sim(32\mu m)^2$ central area ($\sim$2600 spheres) within

the larger crystal domain. Particle motions were observed by microscope, recorded to videotape using a CCD camera and tracked by standard image-processing techniques[31]. In most colloid experiments the important thermodynamic control variable is particle volume fraction. The present experiment achieved substantial variation in sphere diameter using small changes in temperature, which altered thermal energies by less than 1%. In this paper we monitor and report temperature rather than volume fraction because the interactions between spheres contain a soft tail that introduces some ambiguity into the assignment of a geometric diameter to the particles. Below 24°C the system is jammed and no dynamics are observed. Above 27.5°C the in-plane crystals melt. Our primary measurements of the frustrated states probe five temperatures from 24.7°C to 27.1°C in 0.6°C steps. In this range, the hydrodynamic diameter of the nearly-density-matched particles decreases linearly with increasing temperature from 0.89 μm to 0.76 μm (see Fig. S1), while the average in-plane particle separation remains constant (see Table S1). The measured in-plane structures are crystalline. To reach thermal equilibration, the sample was annealed near the melting point before the temperature was slowly decreased. Here "annealed" means the sample was left to evolve for several hours near the melting point to relieve possible unbalanced pressure and provide time for defects to move to produce higher quality crystals. Slow cycling through this temperature range produced no hysteresis.

Anti-Ferromagnetic Order. The images in Fig. 2, A, D show roughly half of the spheres as bright because they are in the focal plane of the microscope; the other half, located near the bottom plate, are slightly out-of-focus and appear dark. A histogram, based on image brightness, showing the degree to which particles are 'up' or 'down' is given in Figure S2 (Supplementary Information). The histogram is bimodal, but clearly a range of 'up' and 'down' is evident in this classical system. The continuous brightness profile was discretized into two 'Ising' states with $s_i = \pm 1$. The brightness cutoff was chosen near the interior minimum so that half the particles are up and half are down. Shifting this cutoff changed structural and dynamical analyses very little, i.e., a few percent, for few percent shifts in up/down cutoff. The nature of the frustrated states can be exhibited in different ways in processed images. One way focuses on the 'bonds' between particles. We refer to pairs of neighbouring particles in opposite states ($s_i s_j = -1$) as satisfied bonds, i.e., satisfying the effective AF interaction, and to up-up or down-down pairs (with $s_i s_j = 1$) as frustrated bonds. Images show that the frustrated bonds form a nearly single-line labyrinth (Fig. 2B) at low temperature that then nucleates into domains (Fig. 2E) at high temperature. Local AF order is alternatively characterized by the average number of frustrated

bonds per particle, $\langle N_f \rangle$. In the limit of weak interactions, an Ising system chooses a completely random configuration with half of the six bonds satisfied and half frustrated, leading to $\langle N_f \rangle = 3$. In the limit of strong interactions, on the other hand, each triangular plaquette has one frustrated bond (Fig. 1A), a third of the bonds are frustrated, and $\langle N_f \rangle = 2$. $\langle N_f \rangle$ is a linear rescaling of the density of excited triangles (3 up or 3 down) in Fig. 2 C, F, which ranges from 0 in the Ising ground state to 0.5 for a random configuration. We find that $\langle N_f \rangle$ decreased from approximately 2.5 to 2.1 in the temperature interval 27.1°C-24.7°C. Detailed statistics of the different local configurations are presented in Supplementary Table S1.

We first consider the static properties of the frustrated samples. In particular we aim to identify similarities and differences between the colloidal system and the Ising model. As the temperature is lowered to increase particle diameter, $\langle N_f \rangle$ is observed to approach 2. This behaviour is expected in the Ising model ground state. However, the vast majority of Ising ground-state configurations are disordered. The colloidal monolayers, by contrast, condense into stripe phases. The stripes are not straight, as could be produced by higher-order interparticle interactions[32]. Rather they bend and form zigzag patterns[22–26] (see Fig. 2A and configuration statistics in Supplementary Table S1). In this colloidal zigzag striped phase, we measured spatial correlations $\Gamma(i-j) = [\langle s_i s_j \rangle - \langle s \rangle^2]/[\langle s^2 \rangle - \langle s \rangle^2]$ over separations $|i-j|$, along the principal lattice directions, of up to 20 particles and found that they decay exponentially in magnitude with alternating sign (Supplementary Fig. S4). $\Gamma(i-j)$ is positive for $i-j$ even and negative for $i-j$ odd. In contrast, $\Gamma(i-j)$ averaged over the Ising ground state is positive when $i-j$ is an integer multiple of 3. Furthermore, for zigzagging stripes each particle has exactly two frustrated neighbours (Fig. 1C), whereas in the fully disordered Ising ground-state N_f can be 0, 1, 2, or 3 (Fig. 1D) and only the average $\langle N_f \rangle$ is 2. These observations suggest that fluctuations in N_f, i.e., $\mathrm{Var}(N_f) = \langle N_f^2 \rangle - \langle N_f \rangle^2$, might be a useful measure for distinguishing the zigzag stripe phase observed here from the disordered Ising ground-state. Figure 3 plots the behaviour of $\mathrm{Var}(N_f)$ as a function of $\langle N_f \rangle$ for the Ising model and for data obtained both from experiments and from hard-sphere Monte Carlo (MC) simulations (Supplementary Information). Results from experiment and simulation agree at both low and high volume fraction and differ from those of the Ising model, especially at high volume fraction wherein interactions are strong. Three length scales affect the physics in this problem: sphere diameter, wall separation, and lattice constant. Therefore, two length ratios can be varied. The simulations showed explicitly (Fig. 3, Fig. S5 (Supplementary Information)) that the frustration behaviors as functions of sphere diameter for different plate separations were similar as long

as the plate separation did not exceed approximately two particle diameters[22,23].

Zigzagging Stripes. Ideal geometrically frustrated systems, such as the AF Ising model, are highly degenerate with extensive entropy at zero temperature. However, in real materials, subtle effects, for example anisotropic interactions[9], long-range interactions[32], boundary conditions[33], and lattice distortions[34–36] relieve frustration. Our partially-ordered zigzag stripe phase at high volume fraction is an example of frustration relief by lattice distortion. In the colloidal monolayer the triangular packing is self-assembled, and the particles are not forced to remain at fixed positions on the lattice[26]. This deformability and the fact that the free volume of the system is a collective function of all particle positions breaks the mapping to simple Ising models with pair-wise additive nearest neighbour interactions. In fact, the positions of the colloidal particles may be thought of as comprising a planar structure that crumples between the two confining planes. This "crumpling" leads to deformations of the planar triangular lattice with satisfied bonds (projected onto the plane) on average $3-4\%$ shorter than frustrated bonds, see Supplementary Table S1. This difference is consistent with the notion that each pair of neighbouring particles prefers to be separated by the *same fixed distance* in 3D, whether or not their connecting bond is satisfied.

A simple tiling argument demonstrates why the colloidal system ground-state configurations of stripes and zigzags pack better than the disordered Ising configurations. The tiling model shows explicitly that maximal volume fractions of stripe and zigzag phases are the same (see Supplementary Information). Each triangular plaquette in the Ising ground-state contains two satisfied bonds and one frustrated bond. Thus, when spheres are close-packed in 3D, the equilateral triangle defined by each such triplet of neighbouring particles is tilted, and when projected onto the 2D plane, it deforms into an isosceles triangle with two short sides along the satisfied bonds and one long side along the frustrated bond (Fig. 4, A, B). Subsequently, close-packed configurations of the buckled spheres in 3D are described by tilings of the plane by isosceles triangles. Figure 4C shows the configurations of isosceles triangles for different numbers of frustrated bonds (N_f) in the basic hexagonal cell. By summing up the angles around the central vertex, one immediately sees that for $N_f = 0$,1,3, the triangles cannot close-pack. Only the two configurations with $N_f = 2$ enable tiling the plane with isosceles triangles, or, equivalently, close-packing of the buckled spheres in 3D. Configuration 2b corresponds to a bend in a stripe, and 2c to a stripe continuing along a straight line. Both have the same maximal volume fraction, thus corroborating observations of zigzagging stripes in the experiments and simulations.

Experiments and simulations indicate a preference for the stripes to form straight segments

rather than to bend easily and thus to generate randomly zigzagging configurations (Fig. 2A). Zigzagging stripes can be viewed as a random stack of ordered lines of alternating up and down particles (Fig. 1C), thus straight and zigzagging stripes are analogous to the face-centred cubic (FCC) lattice and the random hexagonal-close-packed (RHCP) structure[20] in 3D. Straight and zigzagging stripes have the same maximal volume fraction in the close-packed limit. However, for smaller volume fractions there may be an order-by-disorder effect[5,37], giving a small free volume advantage of straight stripes over zigzagging ones, similar to the free volume advantage[38] of FCC over RHCP in 3D. Indeed, stripes in Fig. 2A have a several-particle long persistence length which is more ordered than Fig. 1C.

Instead of an extensive entropy at zero temperature[8], wherein S scales linearly with the number N of particles in the system, the buckled system has subextensive entropy. The number of zigzagging striped configurations grows exponentially with the linear dimension of the system (there are two possible ways of placing one row relative to its predecessor in Fig. 1C), hence the entropy scales[39] as $\sqrt{N}$. Alternatively, a non-branching single-line labyrinth is dictated by $\sim \sqrt{N}$ particles on the boundary, and a cluster of order $\sqrt{N}$ particles should be flipped for the system to rearrange from one zigzag stripe configuration to another. Subextensive ground-state entropy also appears in related models emulating systems with glassy dynamics[40]. Similar zigzag stripes have been observed in superconducting arrays in external fields[41] and in microscopic Ising models[42].

Dynamics. Taken together these observations have interesting consequences for the ground-state dynamics of frustrated systems. The Ising ground-state has a local zero-energy mode, as shown in configuration 3c in Fig. 5A: the central particle can flip without changing the energy of the system, thus rapidly relaxing spin correlations via a sequence of such single spin flips, even at zero temperature. For buckled spheres, on the other hand, the close-packed configurations have only particles with $N_f = 2$, and, moreover, even a particle with $N_f = 3$ in an excited configuration has to cross an energy barrier in order to flip. Thus frustration relief creates a 'glass-like' medium having energy barriers between the various energy minima. Like the glassy behavior of an Ising model on a deformable lattice[43,44], the slow dynamics we observe at low temperature is a consequence of the absence of local zero-energy modes in the bulk.

Online movies (Supplementary Information) permit direct visualization of 'spin flipping' and the motions of thermal excitations and defects in frustrated systems. Thermal excitations labeled as coloured triangles in Fig. 2, C, F were typically found to be generated/annihilated in pairs due to the flipping of a particle shared by the two triangles. Well-isolated thermal excitations, on the other

hand, appear to be more stable. To quantify these effects, we first extract the full time trajectory, $s_i(t)$, of each particle i from the movies. In Fig. 5B we plot the single particle autocorrelation function $C(t) = [\langle s_i(t)s_i(0)\rangle - \langle s_i\rangle^2]/[\langle s_i^2\rangle - \langle s_i\rangle^2]$, averaged over all particles not at lattice defects. As the temperature is lowered, the correlation function develops a stretched exponential form, $C(t) = \exp[-(t/\tau)^\beta]$. The measured relaxation time τ exhibits a dramatic increase as the particles swell at low temperature, while the extracted stretching exponent β decreases, indicating slow dynamics similar to those found in glasses[45].

To further explore the dynamics of different local configurations (defined in Fig. 5A), Fig. 5C shows the measured flipping rate f_r of single particles with a fixed neighbour structure. We measured the probability p that a particle flips between consecutive images given that the Ising states of its neighbours remained unchanged. The time intervals of $dt = 1/30$ sec between frames were short enough such that p was typically small (0.36 at most) and the flip rate could be approximated by $f_r = p/dt$. At high temperature, the behaviour is similar to that of an Ising model undergoing Glauber dynamics: $f_r \sim e^{-\Delta E/k_B T}$ where the energy difference ΔE is proportional to the difference in N_f before and after flipping. As the volume fraction is increased by lowering the temperature, particle dynamics slow by 1-2 orders of magnitude and, more interestingly, *significant differences develop between different geometrical configurations with the same* N_f. Such phenomena may not appear in the simple Ising model where the Hamiltonian depends only on N_f.

Defects in the underlying lattice can strongly affect the properties of frustrated systems. However, detailed knowledge about the role of defects in frustrated systems is very limited. Our experiments permit direct visualization of defects nucleating, annihilating, and diffusing (Supplementary Information movies). By comparing trajectories containing different numbers/types of defects, initial studies suggest that defect particles have enhanced in-plane diffusion (Supplementary Fig.S6) and slower flipping dynamics than those averaged over particles with six nearest neighbours.

Conclusion. We have presented experimental measurements of single-particle dynamics in a geometrically frustrated system. Colloidal spheres with tunable diameter self-assemble to buckled monolayer crystals and form a system analogous to the triangular lattice AF Ising model. By tuning volume fraction, we found that at high compaction, in-plane lattice deformation relieves most frustration and yields a zigzag stripe ground-state with subextensive entropy. The 'free spins' in the Ising ground state are removed; thus the system becomes glassy as the volume fraction is increased. A theoretical analysis shows these features can be captured by a hard-sphere model. We measured spatial correlations and the statistics of various local configurations as well as their

flipping rates and found strong dependences on arrangements of neighbouring particles. As the glassy phase is approached, we observed dramatic slowing of the dynamics and formation of stretched exponential correlation functions. Single-defect dynamics were directly visualized and measured for the first time. Defects have faster in-plane diffusion and slower out-of-plane flipping than the average.

The only other experimental systems offering 'single spin' resolution are based on lithography[10–12]. An attractive feature of the lithographic systems is that any underlying lattice can be created. Colloidal suspensions in 2D, by contrast, will self-assemble into triangular lattices unless an external potential is applied, and since the colloidal system is entirely self-assembling, it possesses a comparatively rich phenomenology originating from lattice deformability. The colloids also offer the possibility for dynamical studies; the lithography-based arrays, by contrast, are frozen in place.

The two-dimensional colloidal frustrated "anti-ferromagnet" we have studied provides an ideal platform for future study of properties of frustrated and glassy systems. Sample dynamics and structure can be microscopically imaged, and the system can be perturbed and manipulated with laser tweezers and other tools. It thus offers hope for deeper insights into the interplay between frustration relaxation and order, e.g., the formation of phases with lower entropy than the anti-ferromagnetic Ising ground state, and into the connections between glassy dynamics, frustration, and sub-extensive yet system-size-divergent entropy. Further experiments to address these issues are readily envisioned. For example, potential energy landscapes for the particles can be created using laser tweezers of varying strength and periodicity (including rigid lattices), enabling experimenters to explore the role of lattice deformability on the dynamics and the creation of structure. Optical tweezers or magnetic traps can also be used to flip and to move individual spins, and video microscopy can be used to probe the resulting system's responses. Boundaries affect frustration, but they are not well studied; such effects could be created by changing sample cell geometry or by fixing particles to the boundary. Gravity, external fields, and surface treatment can be used to mimic the effects of applied magnetic fields on frustrated magnetic systems. Defects affect frustration but have not been explored at the single particle level; such effects can be studied by doping with particles having different shapes and interaction potentials. In the theoretical arena, it will be interesting to consider possible modifications to the rigid-lattice Ising model that generate a zigzagged-stripe ground state, to explore more fully the relation between buckled colloidal systems and the compressible Ising model, including the possibility of generating order out of disorder

via thermal fluctuations, and to study glassy dynamics arising from subextensive zero-temperature entropy.

1. Moessner, R. & Ramirez, A. R. Geometrical frustration. *Phys. Today* **59**, 24-26 (2006).
2. Pauling, L. The structure and entropy of ice and of other crystals with some randomness of atomic arrangement. *J. Am. Chem. Soc.* **57**, 2680-2684 (1935).
3. Harris, M. J., Bramwell, S. T., McMorrow, D. F., Zeiske, T. & Godfrey, K. W. Geometrical frustration in the ferromagnetic pyrochlore $Ho_2Ti_2O_7$. *Phys. Rev. Lett.* **79**, 2554-2557 (1997).
4. Bramwell, S. T. & Gingras, M. J. P. Spin ice state in frustrated magnetic pyrochlore materials. *Science*, **294**, 1495-1501 (2001).
5. Moessner, R. Magnets with strong geometric frustration. *Can. J. Phys.* **79**, 1283-1294 (2001).
6. Ramirez, A. R. Geometric frustration: Magic moments. *Nature* **421**, 483 (2003).
7. Anderson, P. W. The resonating valence bond state in La_2CuO_4 and superconductivity. *Science*, **235**, 1196-1198 (1987).
8. Wannier, G. H. Antiferromagnetism. the triangular Ising net. *Phys. Rev.* **79**, 357-364 (1950); erratum *Phys. Rev. B* **7**, 5017 (1973).
9. Houtappel, R. M. F. Order-disorder in hexagonal lattices. *Physica* **16**, 425-455 (1950).
10. Davidović, D. *et al.* Correlations and disorder in arrays of magnetically coupled superconducting rings. *Phys. Rev. Lett.* **76**, 815-818 (1996).
11. Hilgenkamp, H. *et al.* Ordering and manipulation of the magnetic moments in large-scale superconducting π-loop arrays. *Nature* **422**, 50-53 (2003).
12. Wang, R. F. *et al.* Artificial 'spin ice' in a geometrically frustrated lattice of nanoscale ferromagnetic islands. *Nature* **439**, 303-306 (2006).
13. Möller, G. & Moessner, R. Artificial square ice and related dipolar nanoarrays. *Phys. Rev. Lett.* **96**, 237202 (2006).
14. Nisoli, C., *et al.* Ground state lost but degeneracy found: the effective thermodynamics of artificial spin ice. *Phys. Rev. Lett.* **98**, 217203 (2007).
15. Libál, A., Reichhardt, C. & Reichhardt, C.J.O. Realizing colloidal artificial ice on arrays of optical traps. *Phys. Rev. Lett.* **97**, 228302 (2006).
16. Koshikiya, Y. & Hachisu, S. in *Proceedings of the Colloid Symposium of Japan* (in Japanese, 1982).

17. Pieranski, P., Strzelecki, L., & Pansu, B. Thin colloidal crystals. *Phys. Rev. Lett.* **50**, 900-903 (1983).
18. Van Winkle, D. H. & Murray, C. A. Experimental observation of two-stage melting in a classical two-dimensional screened. *Phys. Rev. A* **34**, 562-1203 (1986).
19. Weiss, J. A., Oxtoby, D. W., Grier, D.G. & Murray, C. A. Martensitic transition in a confined colloidal suspension. *J. Chem. Phys.* **103**, 1180-1190 (1995).
20. Pansu, B., Pieranski, Pi. & Pieranski, Pa. Direct observation of a buckling transition during the formation of thin colloidal crystals. *J. Physique* **45**, 331-339 (1984).
21. Chou, T. & Nelson, D. R. Buckling instabilities of a confined colloid crystal layer. *Phys. Rev. E* **48**, 4611-4621 (1993).
22. Schmidt, M. & Löwen, H. Freezing between two and three dimensions. *Phys. Rev. Lett.* **76**, 4552-4555 (1996).
23. Schmidt, M. & Löwen, H. Phase diagram of hard spheres confined between two parallel plates. *Phys. Rev. E* **55**, 7228-7241 (1997).
24. Zangi, R. & Rice, S. A. Phase transitions in a quasi-two-dimensional system. *Phys. Rev. E* **58**, 7529-7544 (1998).
25. P. Melby *et al.* The dynamics of thin vibrated granular layers. *J. Phys. Cond. Matt.* **17**, S2689-S2704 (2005).
26. Osterman, N., Babič, D., Poberaj, I., Dobnikar, J. & Ziherl, P. Observation of condensed phases of quasiplanar core-softened colloids. *Phys. Rev. Lett.* **99**, 248301 (2007).
27. Alsayed, A. M., Islam, M. F., Zhang, J., Collings, P. J. & Yodh, A. G. Premelting at defects within bulk colloidal crystals. *Science* **309**, 1207-1210 (2005).
28. Han, Y., Ha, N. Y., Alsayed, A. M. & Yodh, A. G. Melting of two-dimensional tunable-diameter colloidal crystals. *Phys. Rev. E* **77**, 041406 (2008).
29. Y. Shokef & T. C. Lubensky, Stripes, zigzags, and slow dynamics in buckled hard spheres, arXiv:0807.3905 (2008).
30. Ogawa, T. A maze-like pattern in a monodispersive latex system and the frustration problem. *J. Phys. Soc. Jpn. Suppl.* **52**, 167-170 (1983).
31. Crocker, J. C. & Grier, D. G. Methods of digital video microscopy for colloidal studies. *J. Colloid Interface Sci.* **179**, 298-310 (1996).
32. Metcalf, B. D. Ground state spin orderings of the triangular Ising model with the nearest and next nearest neighbor interaction. *Phys. Lett. A* **46**, 325-326 (1974).

33. Millane, R. P. & Blakeley, N. D. Boundary conditions and variable ground state entropy for the antiferromagnetic Ising model on a triangular lattice. *Phys. Rev. E* **70**, 057101 (2004).
34. Chen, Z. Y. & Kardar, M. Elastic antiferromagnets on a triangular lattice. *J. Phys. C: Solid State Phys.* **19**, 6825-6831 (1986).
35. Gu, L., Chakraborty, B., Garrido, P. L., Phani, M. & Lebowitz, J. L. Monte Carlo study of a compressible Ising antiferromagnet on a triangular lattice. *Phys. Rev. B* **53**, 11985-11992 (1996).
36. Lee, S.-H., Broholm, C., Kim, T. H., Ratcliff, W. & Cheong S-W. Local spin resonance and spin-peierls-like phase transition in a geometrically frustrated antiferromagnet. *Phys. Rev. Lett.* **84**, 3718-3721 (2000).
37. Villain, J., Bidaux, R., Carton, J. P. & Conte, R. Order as an effect of disorder. *J. Physique* **41**, 1263-1272 (1980).
38. Mau, S. C. & Huse, D. A. Stacking entropy of hard-sphere crystals. *Phys. Rev. E* **59**, 4396-4401 (1999).
39. Liebmann, R. *Statistical Mechanics of Periodic Frustrated Ising Systems* (Springer-Verlag Berlin, Heidelberg, 1986).
40. Nussinov, Z. Avoided phase transitions and glassy dynamics in geometrically frustrated systems and non-Abelian theories. *Phys. Rev. B* **69**, 014208 (2004).
41. Shih, W. Y. & Stroud, D. Two-dimensional superconducting arrays in a magnetic field: effects of lattice structures. *Phys. Rev. B* **32**, 158-165 (1985).
42. Nussinov, Z. Commensurate and incommensurate O(n) spin systems: novel even-odd effects, a generalized Mermin-Wagner-Coleman theorem, and ground states. arXiv:cond-mat/0105253.
43. Chakraborty, B., Gu, L. & Yin, H. Glassy dynamics in a frustrated spin system: the role of defects. *J. Phys. Condens. Matt.* **12**, 6487-6495 (2000).
44. Yin, H. & Chakraborty, B. Entropy-vanishing transition and glassy dynamics in frustrated spins. *Phys. Rev. Lett.* **86**, 2058-2061 (2001).
45. Ediger. M. D. Spatially heterogeneous dynamics in supercooled liquids. *Annu. Rev. Phys. Chem.* **51**, 99-128 (2000).

Acknowledgements We thank Bulbul Chakraborty, Randy Kamien, Dongxu Li, Andrea Liu, Carl Modes, Tai-Kai Ng, Sturart Rice, Yehuda Snir, Tom Witten, and Yi Zhou for helpful discussions. This work is supported by the NSF through the MRSEC grant DMR-0520020 and partially by DMR-0804881.

Author Information Reprints and permission information is available at

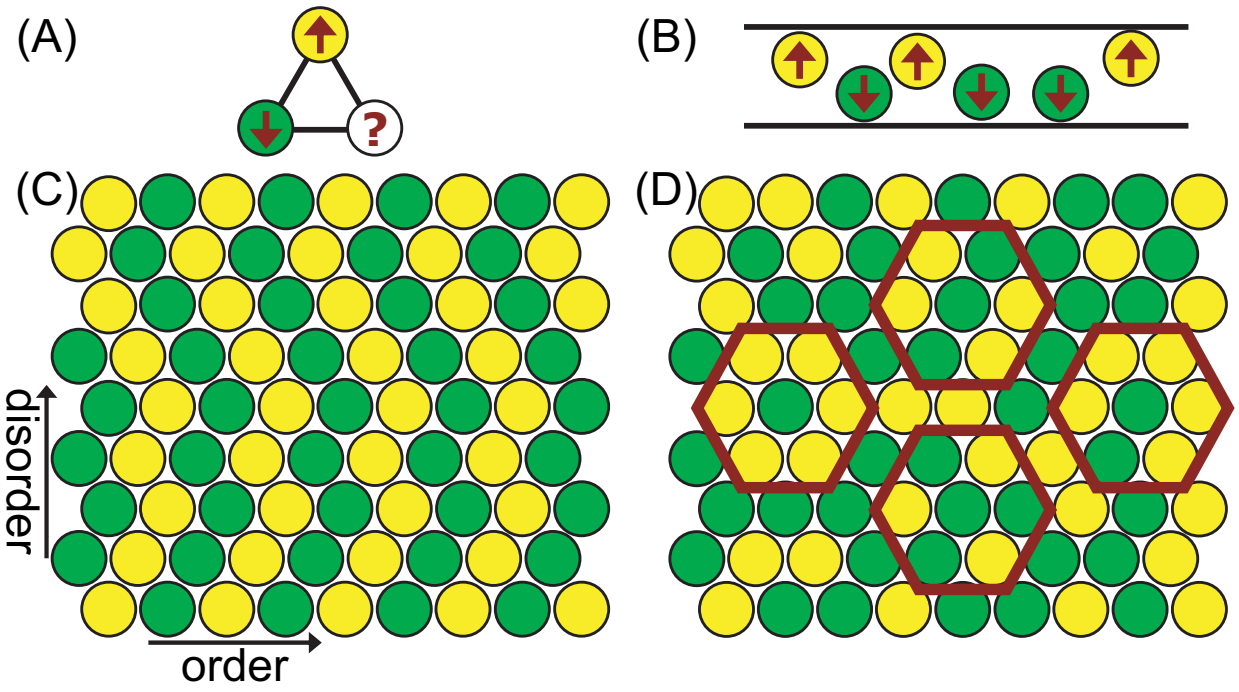

FIG. 1: **Ising ground state.** (A) Three spins on a triangular plaquette cannot simultaneously satisfy all AF interactions. (B) For colloids confined between walls separated of order 1.5 sphere diameters (side view), particles move to opposite walls in order to maximize free volume. (C, D) Ising ground state configurations wherein each triangular plaquette has two satisfied bonds and one frustrated bond. (C) Zigzag stripes generated by stacking rows of alternating up/down particles with random sidewise shifts; all particles have exactly 2 frustrated neighbours. (D) Particles in disordered configurations have 0, 1, 2, or 3 frustrated neighbours (red hexagons).

www.nature.com/reprints. Correspondence and requests for materials should be addressed to Y.S. (yair@sas.upenn.edu) or Y.H. (yilong@ust.hk).

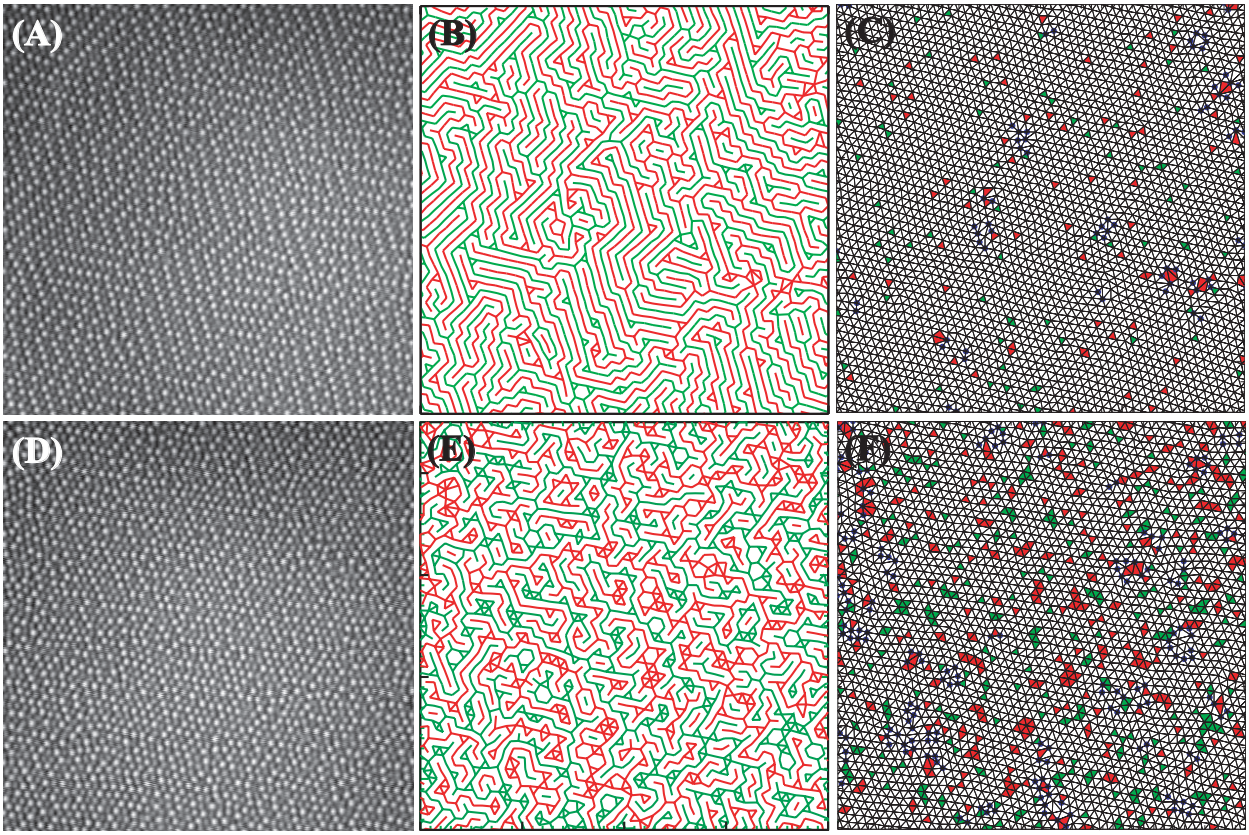

FIG. 2: **Buckled monolayer of colloidal spheres. Movies are in Supplementary Information.** $(32\ \mu m)^2$ area at $T = 24.7°$C (A-C) and $27.1°$C (D-F). (A, D): Bright spheres: up; dark spheres: down. (B, E): Labyrinth patterns obtained by drawing only the frustrated up-up (red) and down-down (green) bonds. (C, F): Corresponding Delaunay triangulations. Blue dots mark defects in the triangular lattice, i.e. particles that do not have exactly six nearest neighbours. Thermally excited triangles with three spheres up/down are labelled by red/green.

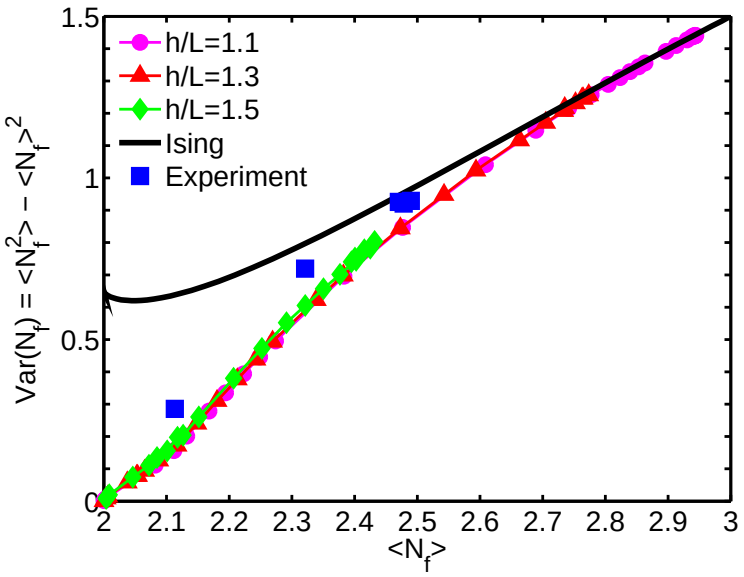

FIG. 3: **Fluctuation in the number of frustrated bonds per particle as a function of its average.** Experiments quantitatively agree with hard-sphere simulations at different plate separations h, normalized by the average in-plane lattice constant L. Simulations collapse onto a single curve and deviate significantly from the behaviour in the Ising model.

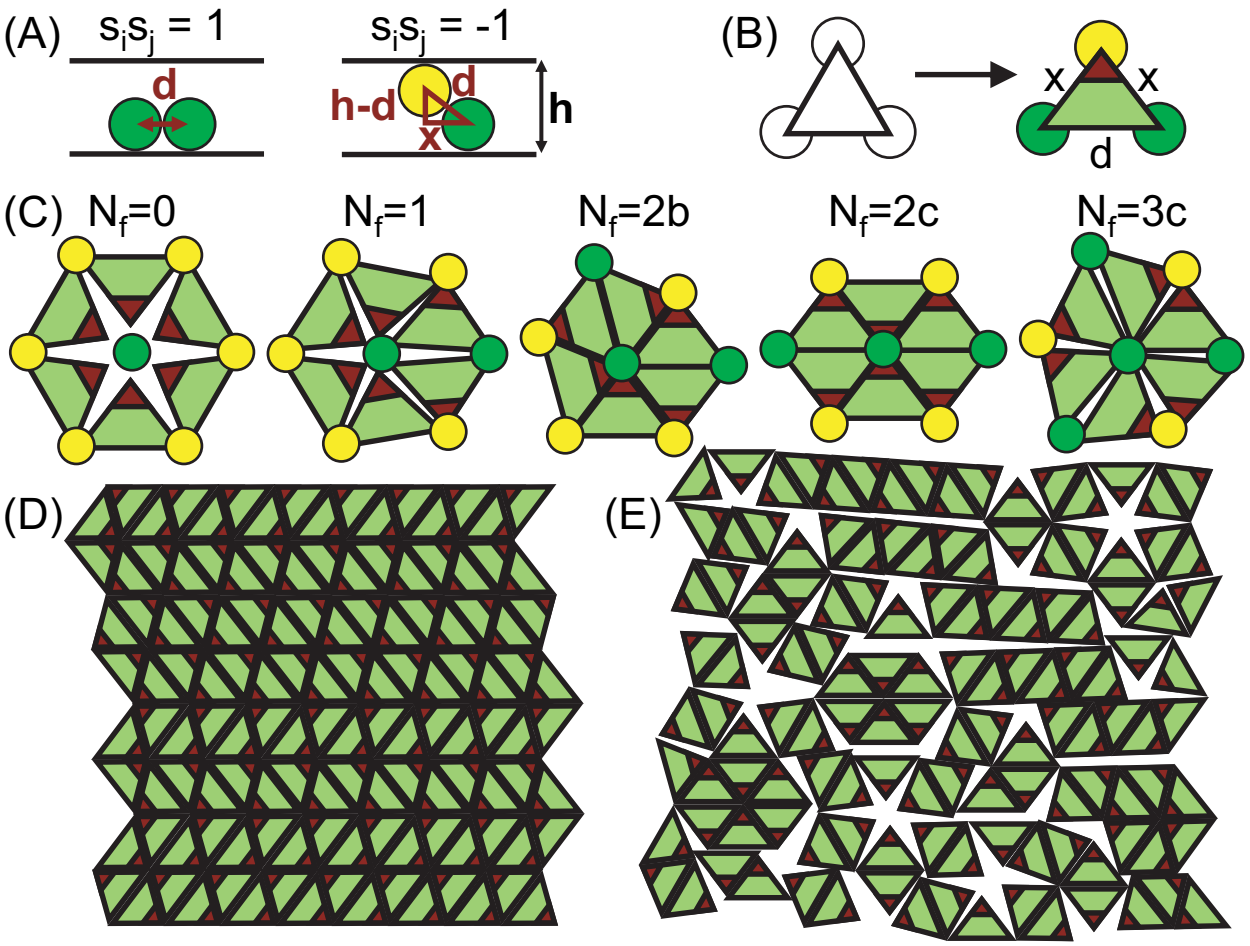

FIG. 4: **Tiling the plane with isosceles triangles.** (A) Close-packed spheres are separated by one particle diameter d in 3D. This distance projected on the 2D plane remains d for a frustrated bond ($s_i s_j = 1$), but is reduced to $x = \sqrt{d^2 - (h-d)^2}$ for a satisfied bond ($s_i s_j = -1$). (B) Viewed from above, each plaquette in the lattice tends to deform to an isosceles triangle with one long side (d) along the frustrated bond and two short sides ($x < d$) along the satisfied bonds. The angle larger than $\pi/3$ is marked in red. (C) All possible in-plane local particle configurations appearing in the Ising ground state. The isosceles triangles can tile the plane without extra space only for $N_f = 2$. The "white space" for $N_f = 0$,1,3 corresponds to additional excluded volume. (D, E) Tilings corresponding to striped and disordered Ising ground-state configurations, respectively, of Fig. 1, C, D.

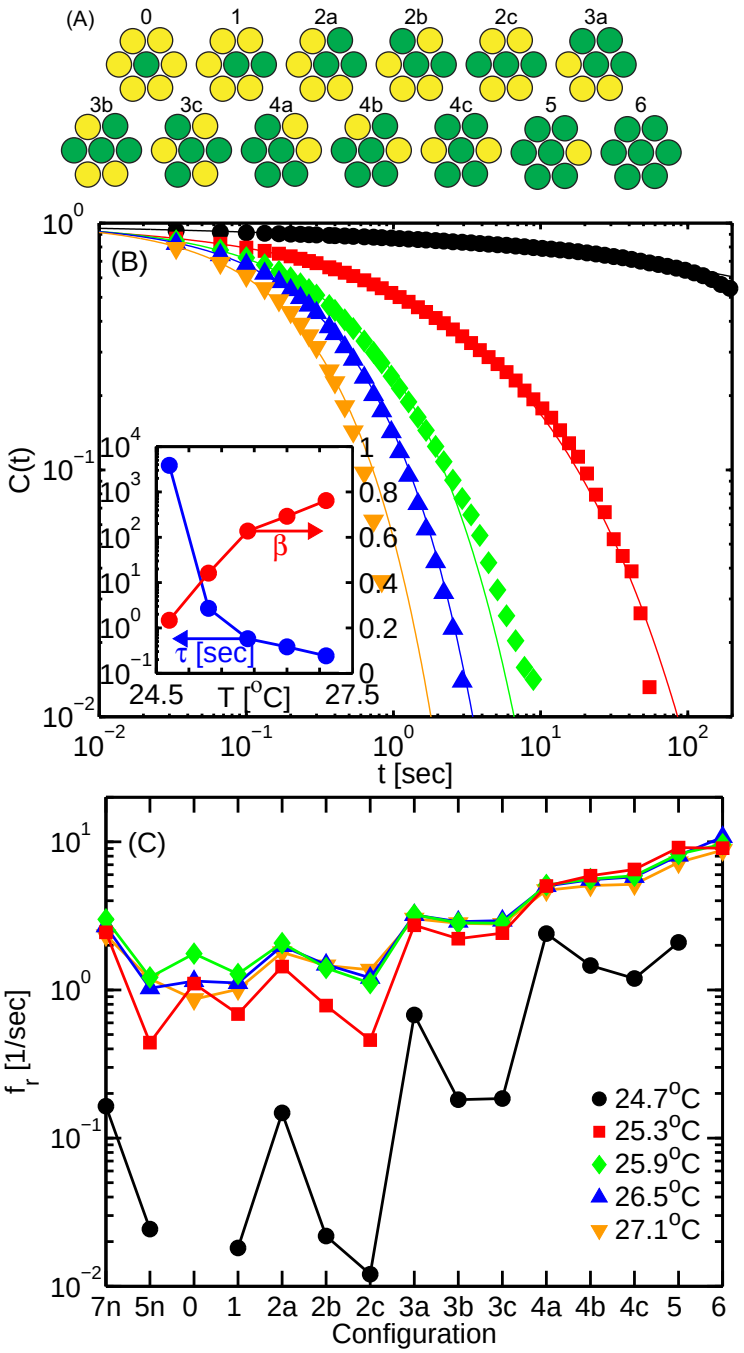

FIG. 5: **Single particle dynamics.** (A) Local configurations are labelled by their value of N_f and an index a,b,c indicating the precise geometrical arrangement of the frustrated neighbours for $N_f = 2, 3, 4$. Symmetry to rotation and inversion reduces the 2^7 possible configurations to the 13 given here. (B) Single particle autocorrelation functions plotted versus decay time. Lines are fits to stretched exponentials $C(t) = \exp[-(t/\tau)^\beta]$, with τ and β given in the inset. (C) Flipping rates for the different local environments. Configurations 7n and 5n are defects in the in-plane lattice, with 7 and 5 nearest neighbours.

Supplementary Information

I. EXPERIMENTAL METHOD

We synthesized micrometer sized NIPA (N-isopropyl acrylamide) microgel spheres by free-radical polymerization[1]. Surfaces of NIPA spheres were crosslinked with PMMA (polymethyl methacrylate) and modified with carboxylate groups. NIPA spheres were suspended in the aqueous buffer solution (pH = 4.0, 20 mM acetic acid). Because more than 90% of the volume of these microgels is water, NIPA spheres have an excellent density match to the water suspension. NIPA polymers become more hydrophobic at high temperature[2], and therefore sphere diameter decreases with increasing temperature as a result of water moving out of the microgel sphere. Figure S1 shows that from $T = 24.5°$C to $28.5°$C, the hydrodynamic diameter, obtained from dynamic light scattering, decreases linearly from 0.90μm to 0.68μm. These measurements also show that sphere size polydispersity is small ($<$3%). The spheres are sterically stabilized: electrostatic interactions are negligible because the surface charge density is very low and the ionic strength is high. A 1.5 μL droplet of colloids will spread over the (18 mm)^2 coverslip area via capillary forces. The cell was sealed with epoxy so that the total volume and number density of the spheres are fixed. The particle number density is virtually constant over the entire sample. It does not change when the particle diameter varies since both total sample volume and total particle number are fixed. The thickness of the sample cell varies from one to several micrometers over the (18 mm)^2 area. Hard spheres form a monolayer triangular lattice, a monolayer buckled phase, two-layer square lattice, etc., at different wall separations[3,4]. We choose an area with cell thickness corresponding to the monolayer buckled phase. In the 38.4×51.2 μm^2 field of view, the thickness variation is $\sim$20 nm, which is much smaller than the sphere diameter, thus walls are effectively parallel. Our temperature controller (Bioptechs) on the microscope has 0.1°C resolution.

The pair potentials $u(r)$ of NIPA spheres were measured from the radial distribution function, $g(r = |\mathbf{r}|)$, in a dilute monolayer with $\sim$10% areal fraction. The radial distribution function is the azimuthal average of the pair correlation function

$$g(\mathbf{r}) = \frac{1}{n^2}\langle \rho(\mathbf{r}' + \mathbf{r})\rho(\mathbf{r}')\rangle, \tag{1}$$

where $\rho(\mathbf{r}) = \sum_{j=1}^{N(t)} \delta(\mathbf{r} - \mathbf{r}_j(t))$ is the distribution of N particles in the field of view and n is the number density. We corrected for image artifacts[5] at each temperature using the method described

in Ref. [6]. From $g(r)$, we applied the liquid structure theory to extract[7,8] the pair potentials, $u(r)$, for example see Fig.1A of Ref.11. The effective radius at $u(r) = 1\ k_BT$ is usually about 12% smaller than the corresponding hydrodynamic radius measured by dynamic light scattering.

A five minute video was recorded at 30 frames/sec for each temperature. The particle in-plane (x, y) positions in each frame were obtained from standard image analysis algorithms[9] with 0.5 pixel = 40 nm spatial resolution. The field of view has a slightly brighter central region under the illumination of the microscope. We measured this non-uniform background and removed it from the particles' brightness profiles. The histogram of particles' brightness has a bimodal distribution as shown in Fig. S2. 48%$\pm$2% of the particles were darker than the central minimum point for all temperatures. The smaller percentage of darker particles is a result of illumination and imaging and not of gravity. Our small Brownian NIPA spheres are very well density matched and the gravitational height $k_BT/mg > 100\ \mu$m is much greater than the cell thickness. Thus we discretize s to 1 and -1 with a 50:50 ratio based on their brightness.

II. NUMERICAL SIMULATIONS

We model the NIPA particles as hard spheres of diameter d confined between parallel hard walls of separation h. We performed 3D Monte Carlo (MC) simulations with two types of time steps, involving either a small displacement of a single particle or a lateral volume-preserving deformation of the simulation box. Due to the hard core nature of the interactions, temperature is irrelevant and each MC move is accepted if there are no sphere overlaps after it. The average lattice constant L is set by the number density and is defined as the nearest neighbour separation the system would obtain had the particles been arranged in a perfect triangular lattice. We typically used $N = 1600$ particles and modified N to verify numerical convergence.

III. TABLE S1 FOR CONFIGURATION STATISTICS

Table S1 gives detailed statistics of the different local configurations defined in Fig. 5A.

IV. OUT-OF-PLANE SPATIAL CORRELATIONS

The spatial correlation of spins is reflected by the spin-spin correlation $\langle s(x,y)s(0,0)\rangle$, and its Fourier transform, the spin-structure factor $\langle|s(q_{xy})s(-q_{xy})|\rangle$. They can be displayed frame by frame as movies or averaged over all frames as shown in Fig. S3. Note that their hexagonal patterns reflect the 6-fold symmetry in particles' spin correlations, not the underlying in-plane lattice. For example, numerically randomizing spins on the same triangular lattice yields no pattern of $\langle s(x,y)s(0,0)\rangle$. Moreover, $\langle s(x,y)s(0,0)\rangle$ appears to be insensitive to the accurate value of s. For example, very similar values for $\langle s(x,y)s(0,0)\rangle$ were obtained by the three following ways: 1) assuming $s(x,y)$ is proportional to the total brightness of the sphere at (x,y); 2) rescaling the bimodally distributed brightness to a uniform distribution; or 3) discretizing s to 1 or -1. The first inner dark hexagonal rings in Fig. S3, A, C, E indicate that nearest neighbours (at separations of one lattice constant L) are anti-correlated. The second bright ring indicates that the next layers of neighbours ($\sqrt{3}L, 2L$) are positively correlated. After averaging over $\sim$9000 frames, Fig. S3, C-F are much smoother than the same individual frames displayed in the movies. This smoothness indicates that the sample explored a large number of configurations during the 5-minute experiments. In contrast, the noisy Fig. S3, A, B, at $24.7°$C suggest that the system was trapped into a more or less glassy state. The video of $T = 24.7°$C shows that most particles were frozen. At even lower temperatures, spheres are almost completely jammed. Discrete dots in Fig. S3C reflect discrete pair separations on the triangular lattice. At higher temperature, particles jiggled more around their lattice sites and smeared out these discrete dots.

Both the mass-density and spin structure factors of an ideal random zigzag-stripe (rzs) state will exhibit Bragg lines analogous to the Bragg rods in the structure factor of the random hexagonal close-packed (rhcp) structure[12]. For the equilateral-to-isosceles distortion we observe, these structure factors are very similar to those of a hexagonal lattice out to about the third ring of reciprocal lattice vectors. Unfortunately, our system does not present ideal rzs order. It has regions of extended straight stripes that are inconsistent with an ideal rzs phase, and it has a sufficient number of defects that the orientational order of stripes of any kind is destroyed. Thus our experiments do not cleanly exhibit Bragg lines.

The above spatial correlation function $\langle s(x,y)s(0,0)\rangle$ as a function of the continuous particle positions is affected by the lattice deformation. In order to isolate the out-of-plane correlations one may wish to map the system onto a perfect triangular lattice and calculate the 'spin' correlation

function on that lattice. We measured correlations as a function of the particles' logical distance $i-j$ along one of the principal directions of the lattice, as shown in Fig. S4. Mapping the particle positions to an undeformed lattice is impossible due to the presence of in-plane topological defects. Nonetheless, we were able to consider pairs of particles i and j such that all particles along the chain connecting them had exactly 6 neighbours. By this procedure the correlation is calculated only between particles in a neighbourhood free of defects.

The experimental results are compared to the ground state of the anti-ferromagnetic (AF) Ising model (black), obtained from a MC simulation on an $N = 100 \times 100$ triangular lattice, and to a phase of stripes that zigzag randomly (cyan). For short distances, correlations in the experiments decay more or less exponentially and they decay more slowly at the lower temperatures. This procedure enables seeing this decay in a clean manner up to a separation of 8 particles for $T = 24.7°\mathrm{C}$ (blue). More importantly, one may clearly see that over the entire separation range considered of 20 particles, the sign of the correlation changes in the $T = 24.7°\mathrm{C}$ experiment in the way it does in the ideal striped phase (with the exception of $|i-j| = 15$ whose value is close to the noise level). This behaviour significantly differs from the Ising model in which the correlation changes sign every 3 particles[13]. For $T = 27.1°\mathrm{C}$ (red) the sign of the correlation appears to vary randomly beyond $|i-j| = 4$ and there is no striped order. As seen in Fig. S4, MC simulations of hard spheres (green and gold) agree with the experiments.

V. GEOMETRIC CALCULATIONS

The maximal particle diameter $d_{\max}$ for a close-packed zigzag stripe configuration may be easily calculated. Such striped configurations correspond to tiling the plane with isosceles triangles. Each triangle has one long side of a length equal to the particle diameter d, and two shorter sides of length $x = \sqrt{d^2-(h-d)^2}$, where h is the separation between the parallel plates confining the spheres. The area of each isosceles triangle is $A = (d/2)\left[x^2-(d/2)^2\right]^{1/2}$. To relate this to the separation L between particles on a perfect triangular lattice, we consider a deformed and an undeformed lattice with the same number density of spheres. This condition may be expressed by equating the areas of the triangular plaquettes in the two structures. In the deformed lattice each plaquette is isosceles with the area given above, whereas in the undeformed triangular lattice each plaquette is an equilateral triangle of side L, and hence area $\frac{\sqrt{3}}{4}L^2$. This leads to the following equation for the maximal sphere diameter in terms of the plate separation h and the undeformed

lattice constant L,

$$d_{\max}^4 - 8hd_{\max}^3 + 4h^2d_{\max}^2 + 3L^4 = 0. \quad (2)$$

We now show that the ratios between the lengths of the frustrated and satisfied bonds in Table S1 are consistent with all neighbouring particles having a fixed 3D distance. Assume each such pair of neighbours is separated a distance ℓ in 3D. For a frustrated bond, both particles are at the same height, hence the projection of this separation onto the 2D plane is $\ell_{\text{frus}} = \ell$. For a bond that satisfies the effective AF interaction, we assume each of the two particles touch the opposite walls, hence their centres have an out-of-plane separation of $h - d$, and, consequently, their separation projected to the plane is $\ell_{\text{sat}} = \sqrt{\ell^2 - (h-d)^2}$. In a close-packed state, the 3D separation becomes equal to the sphere diameter $\ell = d$, hence the projected separation between a satisfied pair is $\ell_{\text{sat}} = x$. This yields the ratio of frustrated to satisfied lengths observed at T=24.7°C by setting $h/d = 1.35$, which is a reasonable value based on the experimental measurements.

VI. SIMULATION RESULTS

We estimate the free volume advantage of zigzag stripes over disordered Ising ground-state configurations by MC simulation. For a given Ising configuration, we fixed the number of buckled spheres but allowed them to rearrange in the plane and then calculated to what extent all particles in each arrangement may be uniformly swelled to diameter $d_{\max}$ without overlapping. Larger $d_{\max}$, therefore, corresponds to better packing. Figure S5 shows that configurations with straight or zigzagged stripes have the same $d_{\max}$ for all sample thicknesses and that these $d_{\max}$ are always much larger than that obtained from disordered configurations.

VII. IN-PLANE DYNAMICS

The in-plane dynamics can be described by the mean square displacement (MSD):

$$\langle \Delta \mathbf{r}_i(t)^2 \rangle = \langle (\mathbf{r}_i(t) - \mathbf{r}_i(0))^2 \rangle. \quad (3)$$

The plateaus of the MSD in Fig. S6A show that particles are caged by their neighbours. Higher plateau values at high temperature indicate that cages are larger at lower volume fraction. Note that the divergence of the MSD at high temperature does not necessarily indicate crystal melting. Particles can jump out of cages by gliding and climbing of dislocations[11]. Fig. S6B clearly shows that defects have larger in-plane motions compared to particles with 6 nearest neighbours.

VIII. ONLINE MOVIES

All movies are in real time at 30 frames/sec.

Movie S1: Raw experimental video at $T = 24.7°$C, corresponding to Fig. 2A.

Movie S2: Labyrinth pattern at $T = 24.7°$C, corresponding to Fig. 2B.

Movie S3: Thermal excitations and defects at $T = 24.7°$C, corresponding to Fig. 2C.

Movie S4: Raw experimental video at $T = 27.1°$C, corresponding to Fig. 2D.

Movie S5: Labyrinth pattern at $T = 27.1°$C, corresponding to Fig. 2E.

Movie S6: Thermal excitations and defects at $T = 27.1°$C, corresponding to Fig. 2F.

---

1. Alsayed, A. M., Islam, M. F., Zhang, J., Collings, P. J. & Yodh, A. G. *Science* **309**, 1207 (2005).
2. Pelton, R. *Adv. Colloid Interf. Sci.* **85**, 1 (2000).
3. Pieranski, P., Strzelecki, L. & Pansu, B. *Phys. Rev. Lett.* **50**, 900 (1983).
4. Schmidt, M. & Löwen, H. *Phys. Rev. Lett.* **76**, 4552 (1996); *Phys. Rev. E* **55**, 7228 (1997).
5. Baumgartl, J. & Bechinger, C. *Europhys. Lett.* **71**, 487 (2005).
6. Polin, M., Grier, D. G. & Han, Y. *Phys. Rev. E* **76**, 041406 (2007).
7. Behrens, S. H. & Grier, D. G. *Phys. Rev. E* **64**, 050401(R) (2001).
8. Han, Y. & Grier, D. G. *Phys. Rev. Lett.* **91**, 038302 (2003).
9. Crocker, J. C. & Grier, D. G. *J. Colloid Interface Sci.* **179**, 298 (1996).
10. Nelson, D. R. *Defects and Geometry in Condensed Matter Physics.* (Cambridge University Press, Cambridge, 2002).
11. Han, Y., Ha, N. Y., Alsayed, A. M. & Yodh, A. G. *Phys. Rev. E* **77**, 041406 (2008).
12. Pusey, P.N., van Megen, W., Bartlett, P., Ackerson, B.J., Rarity, J.G. & Underwood, S.M. *Phys. Rev. Lett.* **25**, 2753 (1989).
13. Stephenson, J. *J. Math. Phys.* **11**, 413-419 (1970).

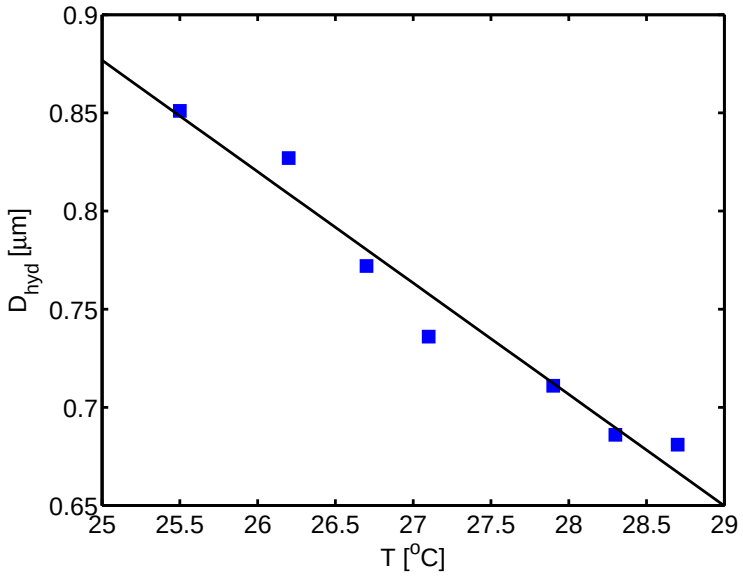

FIG. S1: Temperature dependence of hydrodynamic diameter, obtained from dynamic light scattering.

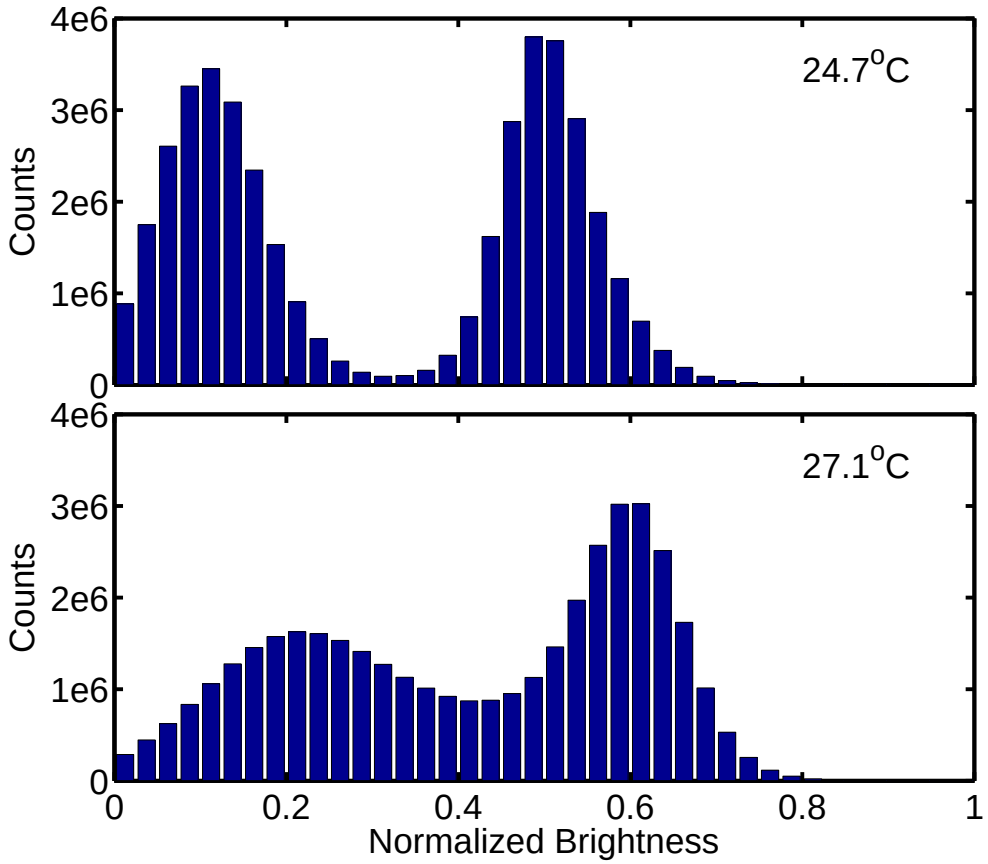

FIG. S2: Histograms of particle brightness normalized to [0,1]. Counts include all particles and all frames of the experimental movies.

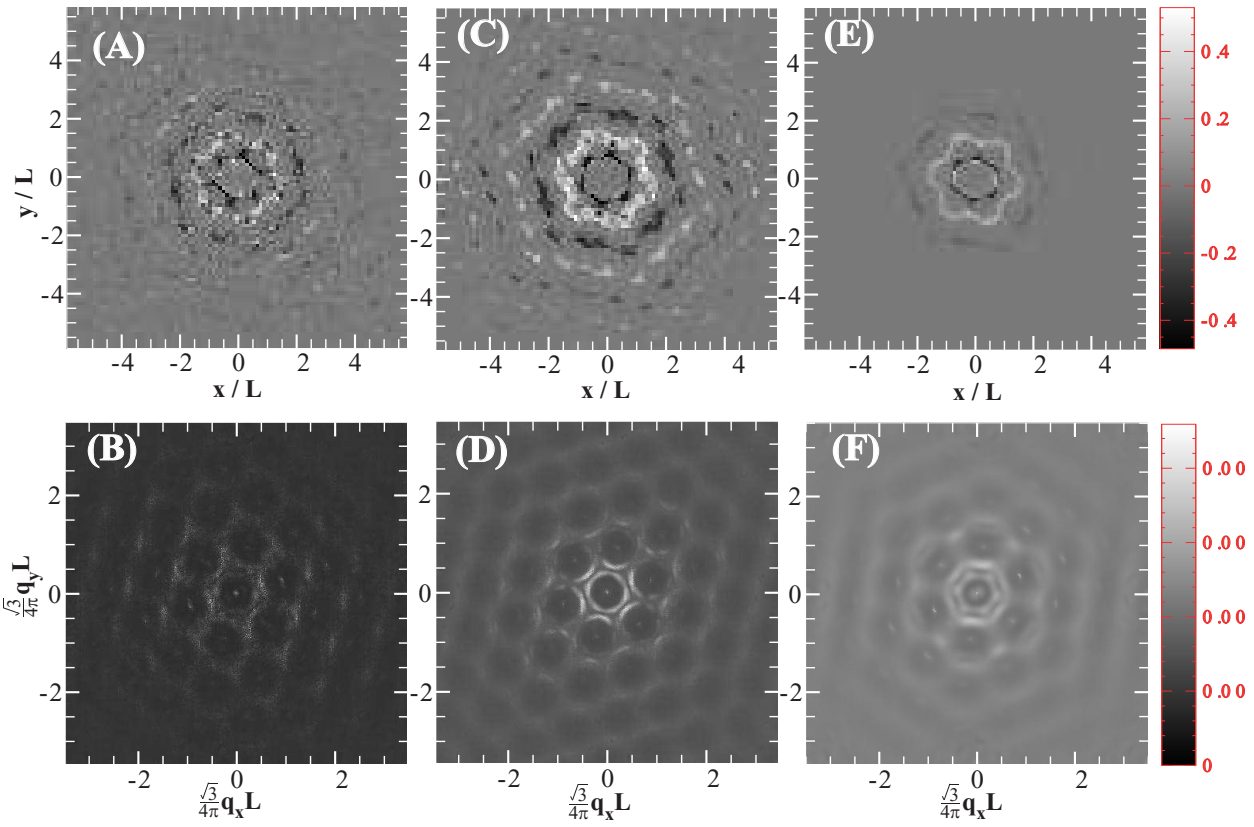

FIG. S3: Static spatial correlations vs the continuous physical distance. (A, C, E): $\langle s(x,y)s(0,0)\rangle$ averaged over ∼9000 frames at T =24.7°C, 25.3°C, and 27.1°C, respectively. Axis unit: lattice constant L. (B, D, F): the corresponding structure factor $\langle|s(q_{xy})s(-q_{xy})|\rangle$ from the Fourier transform of (A, C, E). Axis unit: reciprocal lattice constant $4\pi/(\sqrt{3}L)$. (F) is $3\langle|s(q_{xy})s(-q_{xy})|\rangle$ in order to be bright enough to be visible.

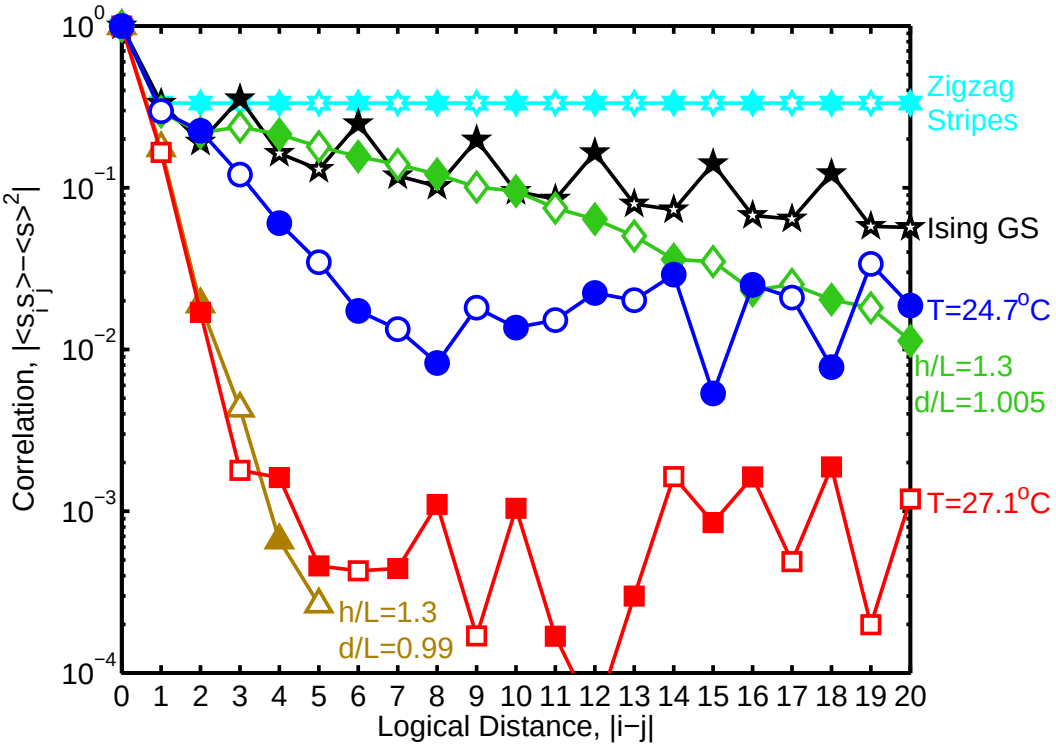

FIG. S4: Static spatial correlations vs the discrete logical distance on the lattice, for experiments, simulations, Ising ground state, and randomly zigzagging striped phase. The magnitude of the correlation is plotted on the semilogarithmic scale and its sign is denoted by solid symbols for $+$ and open symbols for $-$. Simulations given here are for plate separations h, sphere diameters d, and average lattice spacing L, chosen to fit the average number $\langle N_f \rangle$ of frustrated bonds in the experimental data plotted.

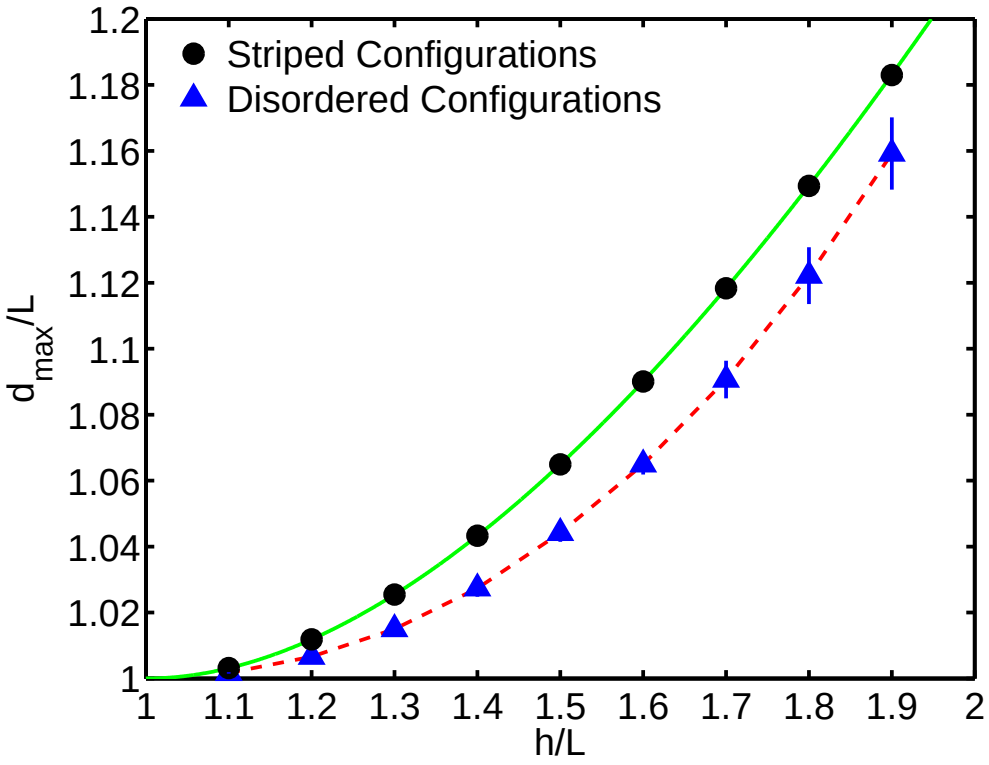

FIG. S5: Maximal particle diameter vs. plate separation. Stripes (straight or zigzagged) pack better than disordered Ising ground-state configurations. The green line is the theoretical prediction based on isosceles tiling. The dashed red line is a guide to the eye for the disordered configurations. Plate separation h and sphere diameter d are here expressed in units of the average in-plane lattice constant L.

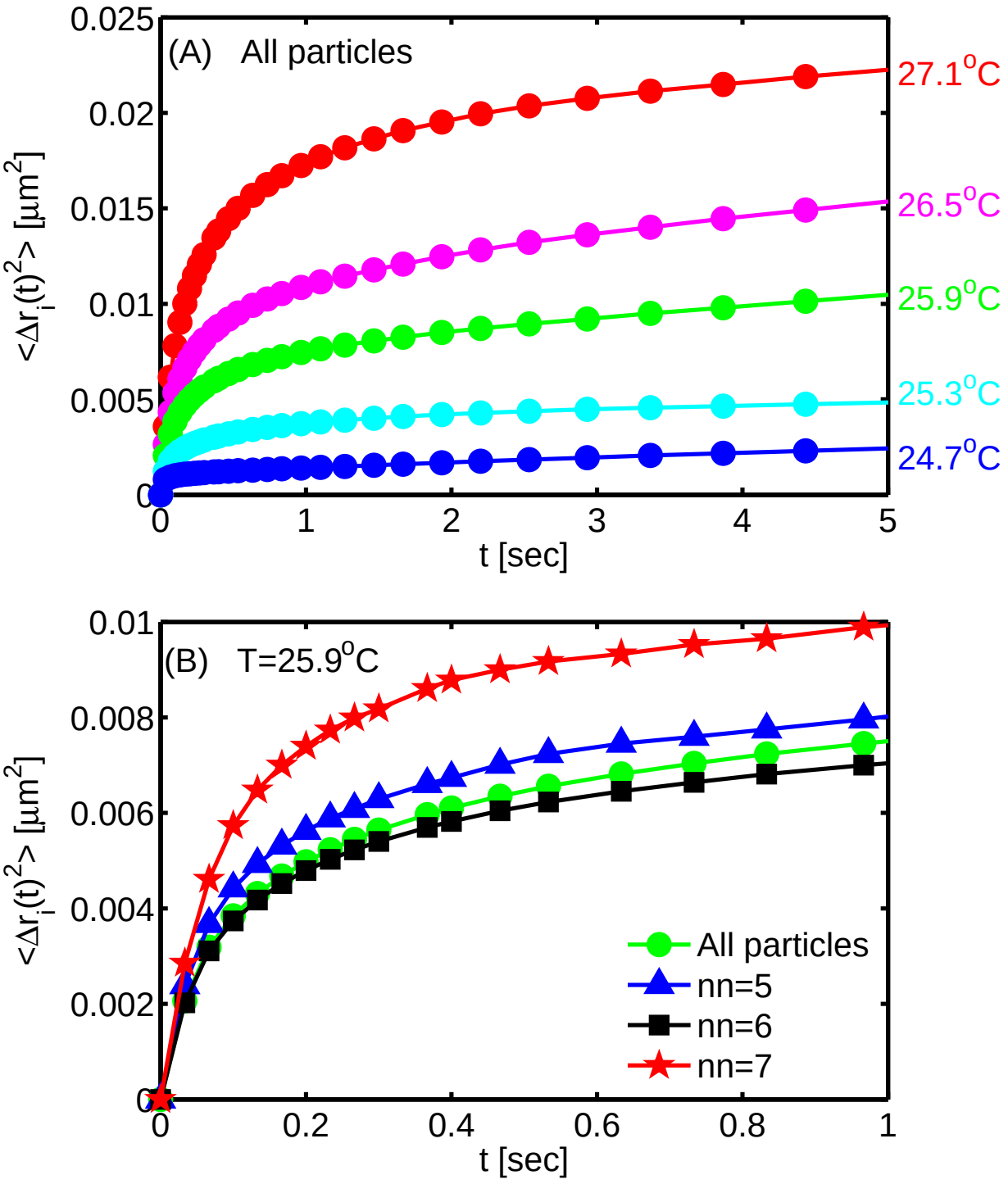

FIG. S6: Mean square displacements. (A) Averaging over trajectories of all particles at the different temperatures. (B) Behaviour of defects at T=25.9°C: all particles (green circles), and particles with 5 (blue triangles), 6 (black squares), and 7 (red stars) nearest neighbours.

	27.1°C	26.5°C	25.9°C	25.3°C	24.7°C	Ising GS	Zigzag Stripes	Random
$nn \neq 6$	5.6	2.8	2.0	1.4	3.2	-	-	-
$N_f = 0$	1.3	1.2	1.2	0.9	0.2	3.3	0	1/64 = 1.6
$N_f = 1$	11.6	12.1	12.2	11.4	7.5	22.3	0	6/64 = 9.4
$N_f = 2a$	7.3	7.2	6.9	4.8	2.7	0	0	6/64 = 9.4
$N_f = 2b$	18.6	19.5	19.9	23.4	33.1	34.9	50	6/64 = 9.4
$N_f = 2c$	9.9	10.8	12.0	22.1	35.0	10.5	50	3/64 = 4.7
$N_f = 3a$	4.8	4.7	4.4	2.5	0.5	0	0	6/64 = 9.4
$N_f = 3b$	20.8	21.1	20.8	18.4	11.4	0	0	12/64 = 19.0
$N_f = 3c$	7.2	7.5	7.5	7.2	5.7	29.0	0	2/64 = 3.1
$N_f = 4a$	2.9	2.8	2.8	1.5	0.1	0	0	6/64 = 9.4
$N_f = 4b$	5.6	5.6	5.5	3.4	0.3	0	0	6/64 = 9.4
$N_f = 4c$	2.7	2.7	2.7	1.7	0.3	0	0	3/64 = 4.7
$N_f = 5$	1.6	1.7	1.8	1.0	0.0	0	0	6/64 = 9.4
$N_f = 6$	0.1	0.1	0.1	0.2	0.0	0	0	1/64 = 1.6
$\langle N_f \rangle$	2.49	2.48	2.47	2.32	2.11	2	2	3
$\langle \psi_6 \rangle$	0.73	0.80	0.87	0.89	0.85	-	-	-
$\langle \ell \rangle_{\text{frus}}$ [nm]	703	706	709	708	700	-	-	-
$\langle \ell \rangle_{\text{sat}}$ [nm]	676	681	686	686	663	-	-	-
L [nm]	676	679	684	685	680	-	-	-

TABLE S1: Percentage of different types of particles averaged over $\sim 10^7$ particles ($\sim$9000 frames), including topological defects ($nn \neq 6$) and non-defects with different numbers N_f of frustrated neighbours. Configurations a,b,c for $N_f = 2, 3, 4$ are defined in Fig. 6A. The three right columns are the theoretical predictions for the Ising ground state, for randomly zigzagging stripes, and for a random state. ψ_6 measures the orientational order of the 2D lattice[10]. $\langle \ell \rangle_{\text{frus}}$, $\langle \ell \rangle_{\text{sat}}$ are the mean frustrated and satisfied in-plane bond lengths. L is the lattice constant measured from the first peak of the radial distribution function.